Invariant Representation and Hierarchical Network for Inspection of Nuts from X-ray Images *

A. Sim and B. Parvin
Imaging Technologies Group, ICSD
Lawrence Berkeley Laboratory
MS 50B-2239
Berkeley, CA 94720

P. Keagy
USDA-ARS
Western Regional Research Center
800 Buchanan St.
Albany, CA 94710

Abstract

An X-ray based system for the inspection of pistachio nuts and wheat kernels for internal insect infestation is presented. The novelty of this system is two-fold. First, we construct an invariant representation of infested nuts from X-ray images that is rich, robust, and compact. Insect infestation creates a tunnel, in the X-ray image, with reduced density of the natural material. The tunneling effect is encoded by linking troughs on the image and constructing a joint curvature-proximity distribution table for each nut. The latter step is designed to accentuate separation of those tunneling effects that are due to the natural structure of the nut. Second, since the representation is sparse, we partition the joint distribution table into several regions, where each region is used independently to train a backpropagation (BP) network. The outputs of these subnets are then collectively trained with another BP network. We show that the resulting hierarchical network has the advantage of reduced dimensionality while maintaining a performance similar to the standard BP network.

1 Introduction

We present a system that has been developed for inspection of pistachio nuts and wheat kernels viewed with an X-ray sensor. The X-ray device reveals internal defects that cannot be otherwise detected by external evidences in the visible domain. Presently, pistachio nuts are inspected for external damages, and a sample of wheat kernels are X-rayed for manual inspection at the mill. In the case of pistachio nuts, we are interested in elimination of aflatoxin contamination[1] [25]. However, there is a strong correlation between contamination

*This work is supported by a grant from U.S. Dept. of Agriculture, under contract number 6053253132, and the Director, Office of Energy Research, Office of Computation and Technology Research, Mathematical, Information, and Computational Sciences Division, of the U. S. Department of Energy under contract No. DE-AC03-76SF00098 with the University of California. This document is LBL-37649.

[1]Aflatoxin is a natural carcinogenic compound, and its concentration is limited by the U.S. and European regulatory agencies.

and insect infestation. And in the case of wheat kernels, we are interested in rejecting those wheat kernels that are infested with maized weevil.

The main novelty of this paper is two fold: First, we derive an *invariant* representation that captures pertinent information on infested as well as non-infested nuts; second, we show that by partitioning this invariant representation, a classifier with reduced dimensionality can be constructed. From a geometric perspective, infestation can be characterized by a dark tunneling appearance in the X-ray image. The tunnel corresponds to the reduced density of the natural content of the nut and to the replacement of that content by a cocoon, insect debris, and air, which have lower X-ray absorption properties. The construction of an invariant representation is complicated by the fact that the tunnel can occur at any spatial location and direction. In the case of pistachio nuts, some air gaps are due to natural separations between the two halves (cotyledons) of the nut meat. And in the case of the wheat kernel, the density of the kernel is reduced near its medial axis.

For pistachio nuts, these natural features may be visible depending upon its resting position. However, the natural separations are generally accentuated by higher contrast than those that are caused by infestation. In this context, our invariant representation first encodes the tunnels and their magnitude, and then parameterizes this representation with respect to location and orientation. Tunnels can be represented in terms of local positive curvature maxima; these local maxima are then linked to form long curve segments. The invariant and compact representation of these curve segments, with respect to rotation and translation, is then encoded by constructing the distribution of local curvature maxima as a function of distance to the outer boundary of the nut. This distribution is a two dimensional joint histogram with the necessary invariant properties.

The second aspect of our work is in the design of the classifier, which is based on the backpropagation network. In general, the corresponding representation for infested nuts is sparse; and our classifier utilizes this property to partition the histogram into several regions, training a network for each region independently, and combining these subnets in a hierarchical fashion. The main benefit is that a classifier with reduced dimensionality (number of weights) than a standard backpropagation network can be obtained.

In the next section, a brief summary of the image acquisition system is given. Then in sections 3 and 4, we outline the details of the invariant representation and classification. In each section, we present the intermediate result of our system followed by examples. Representation of pistachio nuts is a far more complex and interesting problem than the wheat kernels. The paper concludes in section 5 with a summary and a comparison to human performance under similar constraints.

2 Images

In this section, the details of the imaging system for pistachio nuts are covered. The wheat kernels are imaged at higher resolution and a description can be found in [13].
The X-ray images of clean and infested pistachios are captured on photographic film. Nuts from each process stream (Table 2) are individually arrayed on clear adhesive contact paper in one of three orientations (suture plane parallel, perpendicular or at an angle to the film plane) and X-rayed[2]. Films are handled in the dark and exposed without film holders. Twelve bit digital images are obtained from the films at a resolution[3] of $(0.125mm)^2/pixel$. The X-rayed nuts are then opened to determine the presence of insect damage. An image of a clean nut will have the following characteristics: a bright area representing the nut meat, surrounded by a small dark gap between the nut meat and the shell, and a little brighter nut shell outside the kernel. Often there is a dark gap between the two halves of the kernel. The dark areas generally have sharp edges. An insect-infested nut has additional dark areas in the kernel which have been caused by insect bites or tunneling. Figures 1 and 2 show representative images of pistachio and wheat kernels respectively.

(a) (b) (c) (d)

Figure 1: X-ray images of pistachios: (a) & (b) clean and (c) & (d) infested

(a) (b) (c) (d) (e) (f)

Figure 2: X-ray images of wheats: (a), (b) & (c) clean and (d), (e) & (f) infested

[2]90 seconds at 25 keV [0.25 mm Be window] with a Faxitron series X-ray system 4380N, Hewlett Packard, McMinnville, OR; Industrex B film, Eastman Kodak, Rochester, NY

[3]using a Lumiscan 200 film scanner, Lumisys, Sunnyvale, CA

3 Invariant Representation

In this section, we present the details of the invariant representation for the pistachio nuts. Invariant representation, from low level image distribution, has been the subject of many recent efforts [3, 7, 10], where scale space techniques are used to extract significant discontinuities in the form of step and roof edges. In this context, the low level and high level kernels correspond to Gaussian and scaled Gaussian derivatives, respectively. Our views of the invariant representation is that it should address the physical properties of the domain for efficient recognition. In this sense, pure measurements of discontinuities are not sufficient, and further contextual measurements, in the form of proximity to the shell boundary, are required. This will be the essence of the work that will be outlined in this section.

An ideal representation should capture meaningful features with maximum compactness for effective classification. In this context, the low level representations should be rich, stable, and invariant to the rotation and translation of the object in the image plane as well as in the 3-D space. Compactness in representation can be achieved by encoding the low level features so that similar structures at different spatial locations have the same representation. For example, a cocoon on the left or right side of the nut should be represented identically. In our system, the ideal properties of the low level features are captured by computing the surface curvature at each pixel position. Curvature measurements are invariant to translation and rotation, and their positive local maxima identify the positions of troughs. However, other maxima may also be the results of natural surface properties of the pistachio nut such as the split cotyledon. Still, we assert that curvature maxima on the natural surface have higher magnitude, statistically, at a given distance from the nut boundary when these are compared to those curvature maxima, obtained at the identical distance from the nut boundary, that are due to the infestation. Compactness is achieved by parametrizing curvature features as a function of their distance from the boundary of the nut. This parametrization is constructed as a two dimensional histogram that encodes the curvature-distance joint distribution. We suggest that this histogram corresponds to the signature, or a finger print, that can characterize an infested or clean nut, and we present results to that effect. The system architecture is shown in figure 3, and the details of the above computational steps are outlined below.
The tunnels, either due to the natural structure of the object or due to infestation, are localized by grouping local positive curvature maxima, where curvature corresponds to the differential surface properties of the local intensity distribution for the projected image of the tunnel. Curvature is computed from the first and second fundamental forms. These forms uniquely determine certain local invariant quantities of a 3-D surface, where invariance is expressed in terms of translation, rotation, and scaling for X-ray images. Faux and Pratt [6] expressed the first and second fundamental forms in parametric space. However, from a

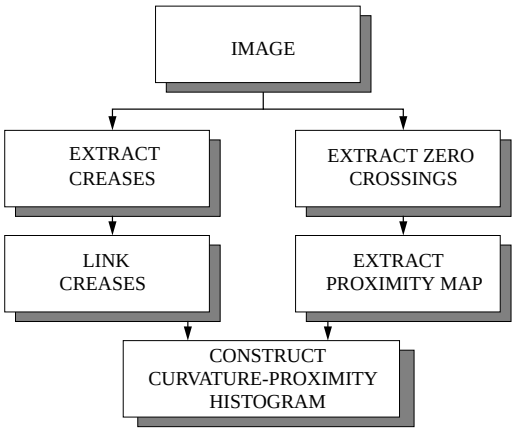

Figure 3: Processing steps

computational perspective, it is desirable to express these forms in Cartesian space. Let a point on the surface be defined as $P = x\vec{i}+y\vec{j}+z\vec{k}$; then the first and the second fundamental forms are computed to be:

$$G = \begin{bmatrix} 1+(\frac{\partial z}{\partial x})^2 & \frac{\partial z}{\partial x}\frac{\partial z}{\partial y} \\ \frac{\partial z}{\partial x}\frac{\partial z}{\partial y} & 1+(\frac{\partial z}{\partial y})^2 \end{bmatrix} \tag{1}$$

$$D = \begin{bmatrix} \frac{\partial^2 z}{\partial x^2} & \frac{\partial z}{\partial x}\frac{\partial z}{\partial y} \\ \frac{\partial z}{\partial x}\frac{\partial z}{\partial y} & \frac{\partial^2 z}{\partial y^2} \end{bmatrix} \tag{2}$$

The normal curvature of a surface is the curvature of the intersecting curve between the surface and the plane containing the surface normal and tangent vector to the curve. The directions in which the normal curvature becomes maximum or minimum are called principal directions corresponding to the principal curvatures. The normal curvature is defined as [6]:

$$K_n = \frac{\dot{X}^T D \dot{X}}{\dot{X}^T G \dot{X}} \quad where\ \dot{X}^T = \begin{bmatrix} \frac{\partial z}{\partial x} & \frac{\partial z}{\partial y} \end{bmatrix} \tag{3}$$

Through elimination and the solution of a pair of simultaneous equations, the following quadratic equation is obtained, where the roots of this equation correspond to maximum and minimum principal curvatures.

$$(g_{11}g_{22} - g_{12}g_{21})k_n^2 - (g_{11}d_{22} + d_{11}g_{22} - 2g_{12}d_{12})k_n + (d_{11}d_{22} - d_{12}d_{21}) = 0 \tag{4}$$

Figure 4 shows the curvature features corresponding to the images shown in figure 1, and figure 5 shows the curvature features corresponding to the images shown in figure 2. On these images, white pixels correspond to troughs (positive curvature maxima) and black pixels to ridges (negative curvature maxima) respectively.

(a) (b) (c) (d)

Figure 4: Maximum principal curvatures of surface intensity for pistachios: (a) & (b) clean and (c) & (d) infested

(a) (b) (c) (d) (e) (f)

Figure 5: Maximum principal curvatures of surface intensity for wheats: (a), (b) & (c) clean and (d), (e) & (f) infested

Once local curvature maxima are determined, they are linked together and long segments are constructed. The steps leading to the extraction of trough segments are similar to previously reported research [7, 10].

1. Smooth the original image with a Gaussian kernel, and compute the curvatures at each pixel on the smooth image,

2. Threshold the curvature image for troughs,

3. Thin the thresholded image using the non-maximal suppression [4] method. The idea is to keep only the troughs whose maximum curvature is the local maximum, and

4. Link the thinned troughs using a hysteresis [4] method. The hysteresis linking method consists of a high and a low threshold. All points above the high threshold are marked as trough points, and similarly, those points below the low threshold are marked as non-trough points. The points between the low and high thresholds can only be traversed from those troughs that are marked by the high threshold.

The result of linking troughs for pistachios and wheats are shown in figure 6 and figure 7. These images are computed with high threshold of 0.99, low threshold of 0.89, and the kernel size of 1.5 for Gaussian smoothing for pistachios, and for wheats, the kernel size of 1.0 is used. These parameters are found to be experimentally appropriate for the nut size, and the expected size of the cocoon that is generated through infestation.

(a) (b) (c) (d)

Figure 6: Result of linking for troughs: (a) & (b) clean and (c) & (d) infested pistachios

(a) (b) (c) (d) (e) (f)

Figure 7: Result of linking for troughs: (a), (b) & (c) clean and (d), (e) & (f) infested wheats

In the next step of the computational process, we compute the distance from each trough point to the boundary of the nut. This is accomplished by first extracting the boundary of the nut with the zero-crossings of the Laplacian of Gaussian (LoG) filter, and then computing the chamfer image. The chamfer image generates a distance map from edges. The map has a zero value on the edge and increases monotonically from the edge. Figure 8 shows the chamfer images obtained from the boundaries of the pistachios nuts shown in figure 1.

(a) (b) (c) (d)

Figure 8: Chamfer images of boundaries of the pistachios: (a) & (b) clean and (c) & (d) infested

Once the proximity map is computed, the two dimensional joint distribution of the curvature-distance table is constructed. Figure 9 shows the cumulative curvature-distance joint histogram for a clean and an infested pistachio, corresponding to the second and the fourth images from example respectively. In figure 9, the distribution indicates that high curvature activities are more localized, at a given distance from the boundary, for clean pistachios than infested pistachios.

In the next section, we show that the joint distribution has the necessary information content to identify the infested nuts in the population.

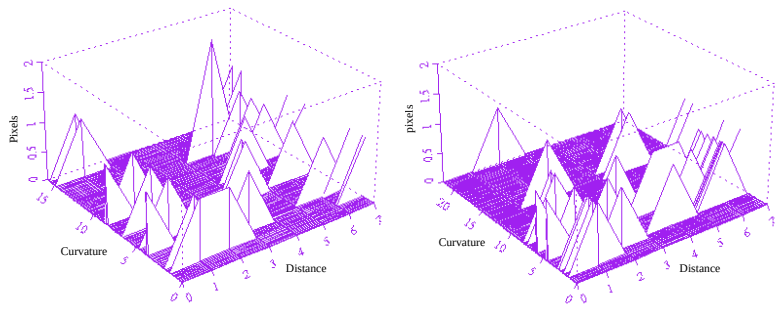

(a) clean nuts (b) infested nuts

Figure 9: Joint histograms of curvature and proximity values

4 Classification

In the design of the classifier, we experimented with several indexing schemes, such as Bidirectional Associative Memory [15] and backpropagation neural network paradigms. The latter consistently produced more favorable results. This is in part due to the large variation in pattern structure and the presence of similar patterns among clean and infested pistachios. The basis for classification is the joint distribution of the curvature-distance table. The curvature values range from 0 to 7.5, and are partitioned into 16 groups, with the distance values ranging from 0 to 9, partitioned into 10 groups. The table is further quantized, as shown in table 1, to reduce the size of the network used for classifying based on the joint distribution and consequently, the size of the training set. The training is based on the backpropagation algorithm. We have experimented with two strategies for further refinement of the classifier design. The first one is the standard backpropagation technique for training a network from a population. In the second approach, we partition the joint distribution table into several regions, where each region is used independently to train a network. These subnets are then trained with another backpropagation network. The backpropagation (BP) algorithm is

		Distances		
		1 2 3 4	5 6 7	8 9 10
Curvatures	1 2 3 4	group 1	group 2	group 3
	5 6 7 8	group 4	group 5	group 6
	9 10 11 12	group 7	group 8	group 9
	13 14 15 16	group 10	group 11	group 12

Table 1: Quantization of joint histogram of the curvature and proximity values

a supervised training technique. In the rest of this section, we first evaluate the performance of a standard BP network, then compare its results with the hierarchical one.

In the standard implementation of the backpropagation algorithm, we use a three layer network and create a sequential array of the joint distribution table as the input to this network. The learning rate and the momentum factor are set at 0.1 and 0.9 respectively. These parameters are selected to maintain a balance between achieving fast convergence and arriving at the desirable local minima. The samples are arranged in different trays, and manually identified as clean or defective nuts. Table 2 tabulates the types of defective pistachio nuts in these trays. The training set consists of a sample of 80 clean and infested pistachio nuts. The clean and infested pistachio nuts are randomly selected from trays M and Q respectively. These nuts were opened to to confirm that they are either clean or infested. Since the nuts are only placed in these trays based on a vague suspicion. We construct three sets of

Product Stream	% of Total Product	Aflatoxin NG/GM	Aflatoxin % of Crop Toxin	Insects per 100 nuts
M	31.06	0	0	0
Q	0.89	89	37	44
A	10.91	1.4	7	2
D	0.13	91	9	9
I	0.53	97	24	13

Tray	Description
M	Good large nuts
Q	Nuts manually removed
A	Nuts with stained shells
D	Lightly stained nuts
I	Small nuts

Table 2: Processing Stream Information

testing data for pistachios. The first and second set have 98 and 100 samples from trays M and Q, respectively. The third set has 452 samples from all the trays. For the classification for wheat kernels, 742 random samples are drawn for training, and another 744 random samples are selected for testing. All samples are selected randomly without replacement, and none of the testing samples are included in the training set. The classification results for pistachios for the backpropagation network with various input size and nodes in the hidden layer are shown in table 3. The poor performance of the third set is due to the presence of other categories of pistachio nuts, as listed in table 2, that in addition of being infested or clean, they may have other defects as well. In a usual agricultural setting, the inspection of pistachio nuts is a multi-stage process, where at each stage, different types of defects or nut grades are inspected. For example, nuts with external defects such as stained shells, are removed by a different inspection system all together. The third set of data was constructed as an experiment to test if the multi-stage inspection and grading process can be reduced into one single stage. Our result indicates that a two class image-based recognition system

is not capable of discriminating different types of defects effectively. For wheats, the classification results with the standard backpropagation network are shown in table 4. The table 4 also shows specific classification results for each infestation category.

Other researchers have explored hierarchical networks for machine vision applications [24] as well. However, our implementation does not use shared weights, nor use more than one hidden layer, and it treats the output of each subnet as a probability measure. Furthermore, the representation used by other researchers is at the pixel level, and no invariant properties of image features are exploited. In our implementation, we divide the joint distribution of the histogram into four or six regions (the number of regions is arbitrary). Each region is then used independently to train a BP network. The results of these subnets are then used as input for the next BP network, as shown in figure 10. The classification results for pistachios with various network sizes are tabulated in table 5. Also, the classification results for wheats with the hierarchical backpropagation network are shown in table 6, along with the results for each infestation category. The result from our hierarchical network approach

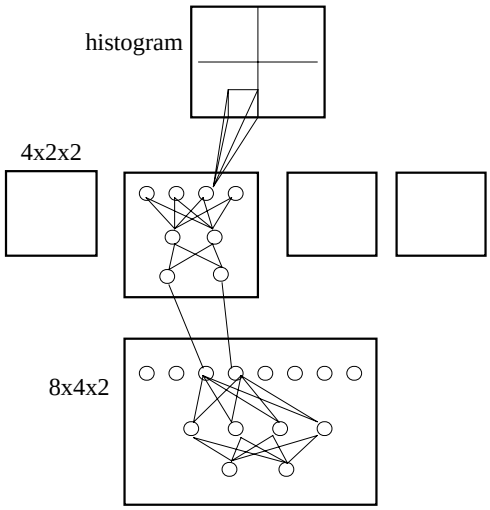

Figure 10: Hierarchical Backpropagation Networks

shows a similar performance to the standard backpropagation network, while reducing the dimensionality. As an example, from the classification results for pistachios, the fourth row (20x5x2, 110 weights) from table 3 and the fifth row (L: 4x2x2, H: 8x4x2, 88 weights) from table 5 indicates that the hierarchical BP network with similar performance to the standard BP network has the reduced dimensionality. The χ^2 test on this example confirms the result as the χ^2 value 6.3185 with 6 degrees of freedom. The reduced dimensionality of the network has the benefit of improved convergence time and a reduction in the number of required training samples.

NODES	WGTS	NTRS	NTES	TPF	FPF
24x12x2	312	80	98	0.80	0.33
			100	0.92	0.22
			452	0.82	0.44
24x6x2	168	80	98	0.88	0.41
			100	0.94	0.24
			452	0.86	0.47
20x10x2	220	80	98	0.73	0.33
			100	0.80	0.18
			452	0.74	0.37
20x5x2	110	80	98	0.80	0.31
			100	0.82	0.24
			452	0.81	0.43
16x4x2	72	80	98	0.78	0.35
			100	0.90	0.28
			452	0.85	0.44
12x4x2	56	80	98	0.63	0.37
			100	0.72	0.30
			452	0.64	0.42

NODES: number of nodes in the networks
WGTS: number of computed weights
NTRS: number of training samples
NTES: number of testing samples
TPF: true positive fraction as the percent of infested nuts actually detected
FPF: false positive fraction as the percent of clean nuts mistakenly identified as infested

Table 3: Performance of standard backpropagation networks on pistachio nuts with varying number of nodes and hidden layers

NODES	WGTS	NTRS	NTES	TPF	FPF
24x6x2	168	742	744	0.79	0.090
			Days	TPF	
			42-45	0.93	
			31-38	0.85	
			21-28	0.65	
20x5x2	110	742	744	0.79	0.071
			Days	TPF	
			42-45	0.91	
			31-38	0.88	
			21-28	0.63	
16x4x2	72	742	744	0.81	0.075
			Days	TPF	
			42-45	0.95	
			31-38	0.89	
			21-28	0.64	

NODES: number of nodes in the networks
WGTS: number of computed weights
NTRS: number of training samples
NTES: number of testing samples
TPF: true positive fraction as the percent of infested nuts actually detected
FPF: false positive fraction as the percent of clean nuts mistakenly identified as infested
Days: the age of infested wheats

Table 4: Performance of standard backpropagation networks on wheat kernels with varying number of nodes and hidden layers

NODES	WGTS	NTRS	NTES	TPF	FPF
L 6x4x2 H 12x8x2	304	80	98	0.71	0.29
			100	0.84	0.26
			452	0.68	0.37
L 6x3x2 H 12x4x2	200	80	98	0.82	0.37
			100	0.86	0.24
			452	0.76	0.45
L 6x2x2 H 12x4x2	152	80	98	0.84	0.33
			100	0.86	0.20
			452	0.66	0.47
L 4x3x2 H 8x4x2	112	80	98	0.80	0.37
			100	0.78	0.26
			452	0.73	0.46
L 4x2x2 H 8x4x2	88	80	98	0.82	0.37
			100	0.84	0.26
			452	0.71	0.38
L 4x1x2 H 8x2x2	44	80	98	0.71	0.22
			100	0.70	0.24
			452	0.59	0.30

NODES: number of nodes in the networks
WGTS: number of computed weights
NTRS: number of training samples
NTES: number of testing samples
L: lower subnetwork
H: upper network
TPF: true positive fraction as the percent of infested nuts actually detected
FPF: false positive fraction as the percent of clean nuts mistakenly identified as infested

Table 5: Performance of hierachical back-propagation networks on pistachio nuts with subnet size of 4 and 6 with varying number of nodes and hidden layers

NODES	WGTS	NTRS	NTES	TPF	FPF
L 6x2x2 H 12x4x2	152	742	744	0.81	0.081
			Days	TPF	
			42-45	0.95	
			31-38	0.85	
			21-28	0.68	
L 4x3x2 H 8x4x2	112	742	744	0.76	0.058
			Days	TPF	
			42-45	0.91	
			31-38	0.86	
			21-28	0.58	
L 4x2x2 H 8x4x2	88	742	744	0.78	0.077
			Days	TPF	
			42-45	0.93	
			31-38	0.82	
			21-28	0.63	

NODES: number of nodes in the networks
WGTS: number of computed weights
NTRS: number of training samples
NTES: number of testing samples
L: lower subnetwork
H: upper network
TPF: true positive fraction as the percent of infested nuts actually detected
FPF: false positive fraction as the percent of clean nuts mistakenly identified as infested
Days: the age of infested wheats

Table 6: Performance of hierachical back-propagation networks on wheat kernels with subnet size of 4 and 6 with varying number of nodes and hidden layers

5 Human Recognition

A human recognition test was conducted using the same training and test sets that were used for training and testing the neural network. Subjects were shown the clean training images and then the infested training images. They were then shown the randomized training set and asked to indicate if the image was clean or infested. The images and responses were reviewed and the subjects were able to examine their errors. This process was repeated with the training images in a different random order. Finally, the subjects gave responses to the two test image sets. Subjects were required to respond clean or infested even if they were unsure. Under these circumstances false positives and false negatives had equal weight. Table 7 presents the results. Detection of infested images (TPF) averaged 90 and 92% while misclassification of clean nuts (FPF) averaged 15 and 18%.

These results suggest that there is sufficient information in the images to detect a large percentage of the insect infested nuts. However, a false positive fraction of 15 to 18% may be higher than pistachio processors can accommodate if this fraction must be discarded. Increasing the degree of certainty required before labeling a nut as infested would decrease the false positive fraction while continuing to identify a reduced but important fraction of the insect infested nuts.

Comparison of human performance in table 7 with network performance in table 5 establishes a benchmark or potential goal for machine performance. Further improvements in machine performance might be achieved by 1) incorporation of additional image features not considered here and/or 2) increasing the confidence level applied to the network output before a nut is labeled as infested.

6 Conclusion

An inspection system for the classification of infested and clean pistachio nuts and wheat kernels is presented. The novelty of this approach lies in the compact and invariant representation of the image features for recognition. The invariance was expresses in terms of the curvature-proximity joint distribution function. Results showed that by partitioning the sparse input array and hierarchical organization of the BP network, the dimensionality in the network could be reduced significantly, without the loss of accuracy. The best network configuration slightly underestimated human performance.

Subject	NTRS	NTES	TPF	FPF
Human 1	80	98	0.90	0.16
		100	0.84	0.14
Human 2	80	98	0.96	0.16
		100	0.98	0.10
Human 3	80	98	0.86	0.18
		100	0.68	0.06
Human 4	80	98	0.96	0.31
		100	0.92	0.24
Human 5	80	98	0.96	0.10
		100	1.00	0.06
Human 6	80	98	0.90	0.18
		100	0.98	0.12
Average	80	98	0.92	0.18
		100	0.90	0.15

NTRS: number of training samples
NTES: number of testing samples
TPF: true positive fraction as the percent of infested nuts actually detected
FPF: false positive fraction as the percent of clean nuts mistakenly identified as infested

Table 7: Performance of human recognitionon on pistachio nuts

References

[1] R. Anan, K. Mehrotra, C. K. Mohan, and S. Ranka. Analyzing images containing multiple sparse patterns with neural networks. *Pattern Recognition*, 26(11):1717–1724, 1993.

[2] E. Baum and D. Haussler. What size net gives valid generalization? *Neural Computation*, 1(1):151–160, 1989.

[3] K. Brunnstrom, J. O. Eklundh, and T. Lindeberg. On scale and resolution in active analysis of local image structure. *Image and Vision Computing*, 8(4):289–296, 1990.

[4] J. F. Canny. A computational approach to edge detection. *IEEE Transactions on Pattern Analysis and Machine Intelligence*, 8(6):679–698, November 1986.

[5] L. V. Fausett. *Fundamentals of neural networks : architectures, algorithms, and applications*. Prentice-Hall, Englewood Cliffs, N.J., 1994.

[6] I. D. Faux and M. J. Pratt. *Computational geometry for design and manufacture*. Ellis Horwood series in mathematics and its applications. Halsted Press, New York, 1979.

[7] L. M. J. Florack, B. M. T. Romeny, J. J. Koenderink, and M. A. Viergever. Scale and the differential structure of images. *Image and Vision Computing*, 10(6):376–389, 1992.

[8] J. M. Gauch and S. M. Pizer. Multiresolution analysis of ridges and valleys in grey-scale images. *IEEE Transactions on Pattern Analysis and Machine Intelligence*, 15(6):635–646, June 1993.

[9] R. C. Gonzalez and R. E. Woods. *Digital image processing*. Addison-Wesley, Reading, Mass., 1993.

[10] L. D. Griffin, A. C. F. Colchester, and G. P. Robinson. Scale and segmentation of grey-level images using maximum gradient paths. *Image and Vision Computing*, 10(6):389–402, 1992.

[11] P. M. Keagy, B. Parvin, and T. F. Schatzki. Machine recognition of naval orange worm damage in x-ray images of pistachio nuts. *Optics in Agriculture, Forestry and Biological*, SPIE Proceedings 2345, 1994.

[12] P. M. Keagy and T. F. Schatzki. Effect of image resolution on insect detection in wheat radiographs. *Cereal Chemistry*, 68(4):339–343, 1991.

[13] P. M. Keagy and T. F. Schatzki. Machine recognition of weevil damage in wheat radiographs. *Cereal Chemistry*, 70(6):696–700, 1993.

[14] P. M. Keagy, T. F. Schatzki, and B. Parvin. Machine recognition of navel orage worm damage in x-ray images of pistachio nuts. *Food Science & Technology/L.V.Y.*, 28, 1996. in press.

[15] B. Kosko. *Neural networks and fuzzy systems : a dynamical systems approach to machine intelligence.* Prentice Hall, Englewood Ciffs, NJ, 1992.

[16] A. D. Kulkarni. *Artificial neural networks for image understanding.* Van Nostrand Reinhold, New York, N.Y., 1994.

[17] S. Y. Kung. *Digital neural networks.* Prentice-Hall information and system sciences series. Prentice-Hall, Englewood Cliffs, N.J., 1993.

[18] L. Lam, S. Lee, and C. Y. Suen. Thinning methodologies - a comprehensive survey. *IEEE Transactions on Pattern Analysis and Machine Intelligence*, 14(9):869–885, September 1992.

[19] S. Lu and A. Szeto. Hierarchical artificial neural networks for edge enhancement. *Pattern Recognition*, 26(8):1149–1163, 1993.

[20] W. K. Pratt. *Digital image processing.* Wiley, New York, N.Y., 1991.

[21] T. F. Schatzki and P. M. Keagy. Effect of image size and contrast on the recognition of insects in radiograms. *Optics in Agriculture*, pages 182–188, 1991.

[22] T. F. Schatzki and P. M. Keagy. Effect of image size and contrast on the recognition of insects in radiograms. *Optics in Agriculture*, SPIE Proceedings 1379:182–188, 1991.

[23] B. W. Silverman. *Density estimation for statistics and data analysis.* Monographs on statistics and applied probability. Chapman and Hall, London, 1986.

[24] S. A. Solla and Y. le Cun. Constrained neural networks for pattern recognition. In P. Antognetti and V. Milutinovic, editors, *Neural networks : concepts, applications, and implementations*, Prentice Hall advanced reference series, pages 142–161. Prentice Hall, Englewood Cliffs, N.J., 1991.

[25] N. F. Sommer, J. R. Buchanan, and R. J. Fortlage. Relation of early splitting and tattering of pistachio nuts to aflatoxin in the orchard. *Phytopathology*, 76:692–694, 1986.

[26] V. Vemuri. Artificial neural networks in control applications. In M. C. Yovits, editor, *Advances in computers*, volume 36, pages 203–254. Academix Press, Inc., Boston, 1993.

List of Figures

List of Tables